An efficient power control strategy for active mitigation of blade in-plane fatigue loading in PMSG-based wind turbines

Safaeinejad, Ali; Rahimi, Mohsen; Zhou, Dao; Blaabjerg, Frede

Published in:
IET Renewable Power Generation

DOI (link to publication from Publisher):
10.1049/rpg2.12923

Publication date:
2024

An efficient power control strategy for active mitigation of blade in-plane fatigue loading in PMSG-based wind turbines

Ali Safaeinejad [1], Mohsen Rahimi [2*], Dao Zhou[3], Frede Blaabjerg[4]

1,2 Department of Electrical and Computer Engineering, University of Kashan, Kashan, Iran

3,4 Department of Energy Technology, Aalborg University, Aalborg DK-9220, Denmark

[1]a.safaeinejad@grad.kashanu.ac.ir

[2]*mrahimi@kashanu.ac.ir

[3]zda@energy.aau.dk

[4]fbl@energy.aau.dk

Abstract

This paper assesses dynamic performance of PMSG-based wind turbine (WT) regarding the blade in-plane fatigue loads once the wind turbine is controlled in power control mode. Blade in-plane oscillations, associated with the poorly blade in-plane modes, can be excited by turbulent winds or grid disturbances that may lead to damage of the blades and reducing the drive-train reliability. To overcome this drawback, at first, a model with three degrees of freedom is extracted for the drive-train system, and then, an active mitigation approach is proposed to mitigate the blade in-plane oscillations. The proposed method can effectively suppress the blade in-plane vibrations by adding a supplementary term into the power control loop that is proportional to the speed difference between the blade and generator. The speed difference between the blade and generator is obtained by estimation of the blade-hub and hub-generator shaft torsional torques. Next, performance of the proposed active mitigation approach is examined by the modal and frequency response analyses and time-domain simulations. Finally, it is shown that the proposed approach has superior performance over the conventional approaches based on the simplified drive-train model and crossing the measured generator speed through a band-pass filter.

Keywords: Blade in-plane oscillations, three-mass drive-train model, PMSG-based WT, blade-hub shaft torsional torque, active mitigating approach

Nomenclature

R	Air density	V_H	Hub height wind speed
ρ	Blades radius	m	Proportionality constant between the spatial and hub height wind speeds
V_w	Spatial average wind speed	$v_{eq_{ws}}$	Equivalent wind speed due to wind shear
$\dot{x}_{nd}$	Tower top displacement speed	$v_{eq_{ts}}$	Equivalent wind speed due to tower shadow
C_p	Power coefficient of the blades	α	Empirical wind shear exponent
λ	Blade tip speed ratio	a	Tower radius
β	Blade pitch angle	X	Blade origin from tower midline

ω_b	Blade angular speed	H	Hub height
$\theta_{sh\text{-}bh}$	Shaft twist angle between the blade and the hub	V_{dc}	dc-link voltage
$\theta_{sh\text{-}hg}$	shaft twist angle between the hub and the generator	C_{dc}	dc-link capacitor
D_{bh}	Mutual damping coefficient between the blades and hub	P_g	Active power injected to the grid
D_{hg}	Mutual damping coefficient between the hub and generator	P_{loss}	Power loss related to the generator, converter and interfaced filter
K_{bh}	Blade-hub shaft stiffness coefficient	I_B	Base current
K_{hg}	Hub-generator shaft stiffness coefficient	i_{gd}, i_{gq}	GSC dq-axes currents
ω_h	Hub angular speed	v_{gd}, v_{gq}	Grid voltages in d-q reference frame
ω_g	Generator angular speed	ω	PLL grid angular frequency
ω_{b_B}	Base angular frequency of the blades	L_g	Interfaced filter inductance
θ_b	Azimuthal angle of the blades	R_g	Interfaced filter resistance
T_t	Turbine torque	$i_{gd,ref}$	Reference of d-axis grid current
P_t	Turbine power	$x_{V_{dc}}$	State variable corresponding to the dc-link voltage controller
T_e	Generator torque	$x_{i_{gd}}$, $x_{i_{gq}}$	State variables corresponding to the grid current controllers
$T_{sh\text{-}bh}$	Torsional torque between the blades and hub	$P_{g,ref}$	Reference active power
$T_{sh\text{-}hg}$	Torsional torque between the hub and generator	k_{opt}	MPPT gain
H_b	Blades inertia constant	x_{P_g}	State variable corresponding to the active power controller
H_h	Hub inertia constant	$\omega_{g,ref}$	Maximum operating of the generator speed
H_g	Generator inertia constant	β_{ref}	Pitch angle command
i_{sd}, i_{sq}	Stator currents in d-q reference frame	τ_β	Time constant of the pitch actuator
v_{sd}, v_{sq}	Stator voltages in d-q reference frame	$k_{P\text{-}\beta}$, $k_{I\text{-}\beta}$	Proportional and integral gains for pitch controller
ψ_{sd}, ψ_{sq}	Stator fluxes in d-q reference frame	x_β	State variable corresponding to pitch controller
ω_s	Stator angular frequency	$\bar{T}_{sh-hg}$	Estimated value of hub-generator torsional torque
ψ_{pm}	Permanent magnet flux linkage	$\bar{T}_{sh-bh}$	Estimated value of the blade-hub torsional torque
L_s	Stator inductance	$\bar{T}_e$	Estimated value of the generator torque
R_s	Stator resistance	ω_n	Cut-off frequency of high pass filters
P_s	Stator output active power	K_E	Feedback gain of auxiliary terms
$i_{sd,ref}$, $i_{sq,ref}$	References of d-q stator currents	ω_t	Angular speed related to the hub and blades in simplified tow-mass drive-train model
α_{i_s}	Closed-loop band width of the stator current control	$x_{i_{sd}}$, $x_{i_{sq}}$	State variables corresponding to the stator current controllers
k_{P-i_s} , k_{I-i_s}	Proportional and integral gains for stator current controllers	A	State matrix
x	Vector of state variables	B	Input matrix
u	Vector of exogenous inputs		

1. Introduction

Due to developments in the wind turbine (WT) industry, recently, new WT manufacturers have concentrated on upscaling of the WTs to megawatt (MW) sizes, resulting in the overall cost

reduction of energy production due to better energy capture [1]. Permanent magnet synchronous generator (PMSG), due to instinct advantages such as brushless structure of the rotor, high efficiency and power density as well as the suitable low-voltage ride-through (LVRT) capability, is a well-known generator type used in large MW size WTs [2]. Figure 1 depicts the WT system with PMSG connected to the distribution grid via back-to-back converters, known as machine-side converter (MSC) and grid-side converter (GSC). In the literature to operate the PMSG-based WTs in power point tracking (MPPT) mode, two control strategies for converters are employed. In the first control strategy, the MSC is used for generator speed/ active power regulation, and the GSC for the dc-link voltage adjustment. In the second control strategy, the MSC is controlled for adjustment of the dc-link voltage, and the GSC for the output active power regulation [2]. In [3], by using the full linearized model of the dc-link dynamics and stability considerations, the dc-link voltage controller in the second control strategy has been designed. Meanwhile, it is shown that the second control strategy provides better LVRT capability than the first control strategy, even under sever 3-phase voltage dip. It is noted that in the most practical cases, the WTs often work in power control mode [4]. Hence, in this paper, the control pattern for the study WT system is established based on the second control strategy.

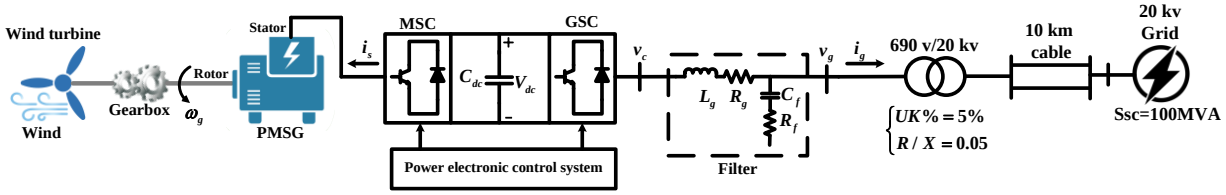

Fig. 1. Schematic diagram of the study grid connected PMSG-based WT

The steadily increasing power rating and structural size in the WTs have led to more susceptible their mechanical rotational parts against dynamic turbulences [2]. This issue brings up a considerable increase in the fatigue loads and stresses on the blades. The WT blades can vibrate as perpendicular or aligned to the rotational plane of the blades, recognized as out-of-plane and in-plane vibrations, respectively. Due to aerodynamic properties of the WT blades, the blade in-plane vibrations exhibit lighter damping feature compared to the out-of-plane vibrations. Hence, blade in-plane vibrations are known as responsible for a significant portion of the operation and maintenance challenges of megawatt-scale WTs [5]. In terms of the motion direction of the blade in-plane loads, their dynamics are strongly coupled to the drive-train system [6, 7]. These modes can be excited by wind speed variations or grid fault conditions that may lead to failure and deformation of blades structure. For mitigating the blade in-plane fatigue loads and preserving the blade structure, further insights into drivetrain dynamics are required. To the best knowledge of the authors, little work has been published in the literature in regard to the integration of the blade flexibilities into the drive-train dynamics and mitigation of the respective loads. In [8, 9], it is shown that to accurately analyze the mechanical rotational parts of the WTs, the dynamics related to blade flexibilities should be incorporated into the drive-train model using the three-mass drive-train model. This model can more efficiently describe the dynamic behavior of the drive-train system, compared to the two-mass drive-train model [10].

Damping methods for rotational mechanical loads are divided into passive and active strategies. Passive methods need additional mechanical equipment with special materials which should be placed on the drive-train structure, but there is a cost associated with this method, and occupies extra space on the drive-train elements [11]. Active damping methods through modification of the control system exhibit more efficient capability and have recently gained much interest [12].

In [13], considering the three-mass drive-train model for a PMSG-based WT, two damping auxiliary components are applied in the control system operated in the speed control mode to suppress both the blade in-plane and drive-train modes. These components are constructed using the measured generator speed signal after crossing through two band-pass filters (BPFs) tuned around the drive-train eigenfrequencies. However, in this paper, the parameters of the drive-train system are considered such that both the drive-train natural frequencies are extracted very close to each other, where not in agreement with actual conditions [8, 14, 15]. Moreover, no elaborated theoretical analysis has been gained for assessing the effect of the proposed damper. It should be noted that the efficacy of the BPFs greatly relies on their parameters and can be compromised under uncertainty presence.

In Refs. [2, 11, 16, 17, 18], it is shown that a damping axillary term proportional to the difference between the rotational speeds of the turbine and generator can present superior performance over the methods based on feeding the generator speed through a BPF with and without considering the model uncertainty. These works are done based on the two-mass drive-train model and the blade flexibilities are ignored, furthermore, the WT operates in the speed or torque control mode .

In solution to the aforementioned deficiencies, this paper presents an efficient active mitigating approach for PMSG-based WT in power control mode to reduce the blade in-plane fatigue loads. This approach is inspired by the active damping methods based on the speed difference between the low-speed and high-speed shafts, with this distinction that the blade flexibilities are considered in the drive-train system.

The innovative contribution of this paper are expressed in the following points: (1) Identifying the drive-train oscillatory modes based on a drive-train model with the appropriate fidelity level and properly respected parameters using the small signal stability analysis (2) Finding out the dynamic correlation between the blade in-plane loads and the rotational speeds in the three-mass drive-train model (3) Modifying the power control loop by adding an auxiliary term proportional to the difference between the rotational speeds of the blade and generator into the power reference (4) Providing the speed difference between the blade and generator by estimation of the blade-hub and hub-generator shaft torsional torques (5) Comparing the efficacy of the proposed active mitigating approach with those of approaches based on the generator speed feedback and the simplified two-mass drive-train model

2 .PMSG-based WT model

This section deals with modelling of aerodynamic part, drive-train system and generator in PMSG-based WTs.

2.1. WT aerodynamic model

To describe the aerodynamic characteristics of an upwind turbine, the aerodynamic conversion process should be considered. The mechanical power extracted by turbine can be given as [19]:

$$P_t = \frac{1}{2}\rho\pi R^2 (V_w - \dot{x_{nd}})^3 C_p(\lambda, \beta) \tag{1}$$

where ρ is the air density, R is the radius of blades, V_w is the spatial average wind speed and $\dot{x_{nd}}$ is the tower top displacement speed; C_p is the power coefficient of the blades which is relevant to construction properties of wind turbine and is defined as a function of the tip speed ratio, λ, and blade pitch angle, β. λ as the blade tip speed ratio is given by

$$\lambda = \frac{R\omega_b}{(V_w - \dot{x_{nd}})} \tag{2}$$

where ω_b is the blade angular speed.

Blade passing phenomenon (BPPh) in three-bladed wind turbines originates from the inherent aerodynamic characteristic of the wind turbine and causes the periodic fluctuations emerged on the mechanical torque. These fluctuations have the frequency content corresponding to the three times the rotational frequency of the blades (p); In other words, the BPPh is generally known as 3p effect [16]. The BPPh consists of the wind shear and tower shadow where the wind shear refers to the spatial distribution variations of the wind speed from upward position to downward position of the blades, while the tower shadow is due to altering the uniform flow of the wind when each of blades encounters the tower. In order to apply the 3p effect in aerodynamic system, the oscillating term related to the mechanical torque is given by [20, 21]

$$\tilde{T_t} = \frac{2}{mV_H}\left[v_{eq_{ws}} + v_{eq_{ts}} + (1-m)V_H \right] T_{t_0} \tag{3}$$

$$V_w = mV_H \tag{4}$$

where m is the proportionality constant between spatial wind speed, (V_w) and hub height wind speed, (V_H), T_{t_0} is the average value of the mechanical torque, $T_{t_0} = P_{t_0} / \omega_{b_0}$, $v_{eq_{ws}}$ is the equivalent wind speed due to wind shear, and $v_{eq_{ts}}$ is the equivalent wind speed due to tower shadow, which their formulas are expressed as

$$v_{eq_{ws}} = V_H \left[\frac{\alpha(\alpha-1)}{8} (\frac{R}{H})^2 + \frac{\alpha(\alpha-1)(\alpha-2)}{60} (\frac{R}{H})^3 \cos 3\theta_b \right] \tag{5}$$

$$v_{eq_{ts}} = \frac{mV_H}{3R^2} \sum_{b=1}^{3} \left[\frac{a^2}{\sin^2\theta_b} \ln(\frac{R^2 \sin^2\theta_b}{X^2} + 1) - \frac{2a^2R^2}{R^2\sin^2\theta_b + X^2} \right] \tag{6}$$

Where α is empirical wind shear exponent, a is the tower radius, X is blade origin from tower midline, H is hub height and θ_b is azimuthal angle of the blades. Hence, the comprehensive

mechanical torque equation, comprising both the average value term (T_{t0}) and the oscillating term ($\tilde{T}_t$), can be given as

$$T_t = T_{t_0} + \tilde{T}_t \tag{7}$$

2.2. Drive-train modelling

The wind turbine drive-train is responsible for transmitting the aerodynamic torque which is derived by blades to the generator's shaft or namely via this system the lift forces extracted from the blades is converted to the electricity energy. This system generally comprises the horizontal axis blades, hub, low speed shaft (LLS), three-stage gearbox, high speed shaft (HSS) and generator. Drive-train system is generally modeled through a collection of rotating masses by shafts [10]. In this modelling method, it is assumed the masses possess inertia without stiffness, whereas the shafts possess stiffness without inertia. The number of masses and shafts of the drive-train model depends on the type of the study drive-train system and required accuracy of dynamic analysis associate with it. The fatigue local loading of the blades are related to edgewise bending modes, whereas bending modes of the blades are generally recognized in the rotor plane. Hence, the referred blade edgewise bending modes on this plane are known as blade in-plane modes. Since the symmetrical in-plane modes of the blades are responsible for motion of the blades in rotational direction, therefor, they can be coupled with the drive-train [22]. In Fig. 2 the symmetrical in-plane modes of the blades are shown wherein all the blades vibrate collectively in the specified direction [23]. In order to study the blade in-plane modes, the blades should be considered as separate mass in the drive-train system model [24]. Using this model, the symmetrical in-plane modes of the blades are coupled to the drive-train and can be observable. Hence, the three-mass drive-train model realizing this aim is employed in this paper.

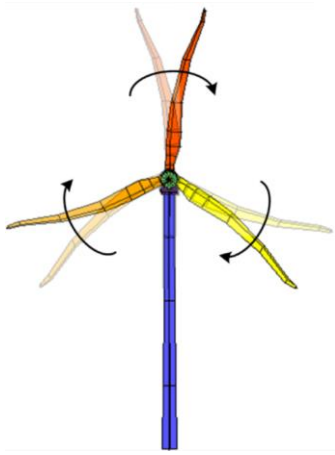

Fig. 2. Symmetrical in-plane modes of the blades [23]

In the three-mass drive-train model, the rotor is split in two masses, the blades and the hub masses, and the third mass is related to the generator. The three-mass drive-train model referred to the HSS is illustrated in Fig. 3 and the linearized form of its dynamic equations are given in (8)-(14).

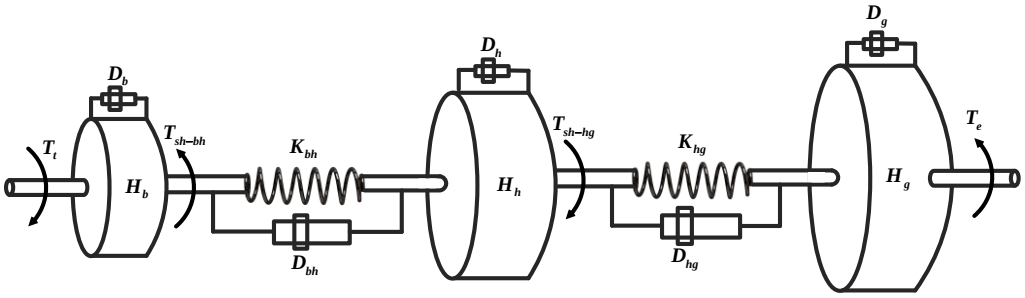

Fig. 3. Three-mass drive-train model

$$\Delta T_t - \Delta T_{sh-bh} - D_b \Delta\omega_b = 2H_b \frac{d\Delta\omega_b}{dt} \tag{8}$$

$$\Delta T_{sh-bh} - \Delta T_{sh-hg} - D_h \Delta\omega_h = 2H_h \frac{d\Delta\omega_h}{dt} \tag{9}$$

$$\Delta T_{sh-hg} + \Delta T_e - D_g \Delta\omega_g = 2H_g \frac{d\Delta\omega_g}{dt} \tag{10}$$

$$\Delta T_{sh-bh} = K_{bh}\Delta\theta_{sh-bh} + D_{bh}(\Delta\omega_b - \Delta\omega_h) \tag{11}$$

$$\Delta T_{sh-hg} = K_{hg}\Delta\theta_{sh-hg} + D_{hg}(\Delta\omega_h - \Delta\omega_g) \tag{12}$$

$$\frac{d\Delta\theta_{sh-bh}}{dt} = \omega_B(\Delta\omega_b - \Delta\omega_h) \tag{13}$$

$$\frac{d\Delta\theta_{sh-hg}}{dt} = \omega_B(\Delta\omega_h - \Delta\omega_g) \tag{14}$$

where the prefix Δ denotes the small deviation around the operating point, ω_h and ω_g are the rotational speeds of the hub and generator, in (p.u.), respectively, $\theta_{sh\text{-}bh}$ and $\theta_{sh\text{-}hg}$ are the shaft twist angles between the blade and the hub and also between the hub and the generator, in (p.u.), respectively, T_t and T_e are the torques related to the turbine and generator, in (p.u.), respectively, and $T_{sh\text{-}bh}$ and $T_{sh\text{-}hg}$ are the torsional torques related to the blade-hub and hub-generator shafts, in (p.u.), respectively, H_b, H_h and H_g are the inertia constants associated to the blades, hub and generator, in (sec), respectively, K_{bh} and K_{hg} are the shaft stiffness coefficients associated to the blade-hub and hub-generator shafts, in (p.u./elec. rad), respectively, D_{bh}, D_{hg} are the mutual damping coefficients between the blade and hub and between the hub and generator in (p.u.), respectively, D_b, D_h and D_g are the self-damping coefficients associated with the blade, hub and generator in (p.u.), respectively, ω_B is the base angular electrical frequency in (rad/sec).

The turbine torque is considered as $T_t=P_t/\omega_b$ and its linearized form around the turbine operating speed ω_{b_0} is obtained as

$$\Delta T_t = \left(\frac{T_{t_0}}{V_{w_0}}\left(3 - \frac{\lambda_0}{C_{p_0}}\frac{\partial C_p}{\partial\lambda}\right)\right)\Delta V_w + \left(\frac{T_{t_0}}{C_{p_0}}\frac{\partial C_p}{\partial\beta}\right)\Delta\beta + \left(\frac{R\omega_{bB}}{V_{w_0}C_{p_0}}T_{t_0}\frac{\partial C_p}{\partial\lambda} - \frac{T_{t_0}}{\omega_{b_0}}\right)\Delta\omega_b \tag{15}$$

where T_{t_0}, V_{w_0}, λ_0 and C_{p_0} are the turbine torque, wind speed, blade tip speed ratio and power coefficient at the operating point, respectively, and ω_{b_B} is the base angular frequency of the blades.

In the three-mass drive-train model, from the blade in-plane fatigue loading point of view, the blade-hub shaft torsional torque, $T_{sh\text{-}bh}$, is considered as blade in-plane bending moment. Hence the oscillations of $T_{sh\text{-}bh}$ is assumed as undesirable torque vibrations, representing the blade in-plane bending fatigue loading. These oscillations may be appeared on the $T_{sh\text{-}bh}$ under wind speed changes or grid faults [25]. In other words, the mechanical and electrical step loads because of including the all frequencies can excite the natural frequency of the blade in-plane modes, and accordingly the blades vibrate with their own resonance frequency [26]. Using 8 to 14, the resonance frequencies of three-mass drive-train model are obtained as

$$f_{1,2} = \frac{1}{2\pi}\left[\frac{-b}{2} \pm \frac{\sqrt{b^2 - 4c}}{2}\right]^{\frac{1}{2}} \tag{16}$$

where b and c in (16) are given by

$$b = -\left[K_{bh}\omega_B\left(\frac{1}{2H_b} + \frac{1}{2H_h}\right) + K_{hg}\omega_B\left(\frac{1}{2H_g} + \frac{1}{2H_h}\right)\right] \tag{17}$$

$$c = K_{bh}K_{hg}\frac{\omega_B}{4}(H_b + H_h + H_g)$$

Therefore, the three mass drive-train model has two resonance frequencies and these resonance frequencies for the study WT system with parameters of Appendix are obtained as $2\pi\times2.29$ rad/sec and $2\pi\times13.34$ rad/sec. The study system is based on the NREL 5MW WT model given in [15]. Since the NREL drive-train is based on the two-mass model, to develop it to the three-mass model, the NREL drive-train parameters are slightly modified according to [14, 27, 28].

2.3. PMSG modelling

This section deals with the dynamic modeling of the PMSG in the rotor reference frame rotating at the generator speed, in which the d-axis is aligned with the rotor flux vector, and the q-axis is perpendicular to it. In PMSG modelling procedure, the following assumptions are considered: (a) positive direction for the stator current, as depicted in Fig. 1, is assigned into the generator, (b) all system parameters and variables are in per unit (c) the PMSG under study is non-salient pole. The stator voltages, fluxes, and electromagnetic torque in the synchronous d-q frame are given by [29]:

$$v_{sdq} = R_s i_{sdq} + j\omega_g \psi_{sdq} + \frac{1}{\omega_B}\frac{d\psi_{sdq}}{dt} \tag{18}$$

$$\psi_{sdq} = L_s i_{sqd} + \psi_{pm} \tag{19}$$

$$T_e = \psi_{pm} i_{sq} \tag{20}$$

Where ψ, v and i are the flux, voltage, and current, in (p.u.), and subscript s denotes the stator quantities. L_s and R_s are the stator inductance and resistance, in (p.u.), respectively, ψ_{pm} is the amplitude of the flux linkage in the stator due to permanent magnet of the rotor, in (p.u.), ω_g is the

electrical rotational speed of the generator, in (p.u.), and it at the steady state condition is equal to the stator angular frequency, ω_s.

under the steady state condition and by ignoring the stator loss, the stator output active power can be written as [3]

$$P_s = -\psi_{pm}\omega_g i_{sq} \tag{21}$$

According to (20) and (21), the electromagnetic torque and consequently the stator output active power can be controlled by the q-component stator current, i_{sq}.

3. Control structure of PMSG-WT

In the following, control structure of the power converters and the pitch system are presented.

3.1. Control structure of the MSC

This section deals with the control loops of the MSC. The main function of the MSC is to adjust the dc-link voltage through regulating the stator output active power. The MSC control structure, comprises the inner dq-axes stator current control loops and outer dc-link voltage control loop.

3.1.1. Inner current control loops of the MSC

By using (18) and (19), the PMSG stator dynamics in terms of the stator current and permanent magnet flux are describe as

$$v_{sd} = R_s i_{sd} + \frac{L_s}{\omega_B}\frac{di_{sd}}{dt} - \omega_g L_s i_{sq} \tag{22}$$

$$v_{sq} = R_s i_{sq} + \frac{L_s}{\omega_B}\frac{di_{sq}}{dt} + \omega_g L_s i_{sd} + \omega_g \psi_{pm} \tag{23}$$

Based on above equations, the closed -loop control of the dq-axis stator current with PI controller is achieved as depicted in Fig. 4. The reference of q-component stator current, $i_{sq,ref}$, for the inner current control loop is determined by the outer dc-link voltage controller, and thus in order to achieve the maximum torque per current, the reference of the d-component stator current $i_{sd,ref}$ is set to zero [3]. In order to determine the parameters, the zero-pole cancelation method is employed. Considering Fig. 4, the following relation is concluded

$$\frac{k_{I-i_s}}{k_{P-i_s}} = \frac{R_s\omega_B}{L_s} \tag{24}$$

After cancelling the pole of the plant with the zero of the PI controller, the closed-loop band width of the stator current control is obtained, as $\alpha_{i_s} = \frac{k_{P-i_s}\omega_B}{L_s}$, and transfer function from $i_{sq,ref}$ to i_{sq} can be given as

$$\frac{i_{sq}}{i_{sq,ref}} = \frac{\alpha_{i_s}}{s + \alpha_{i_s}} \tag{25}$$

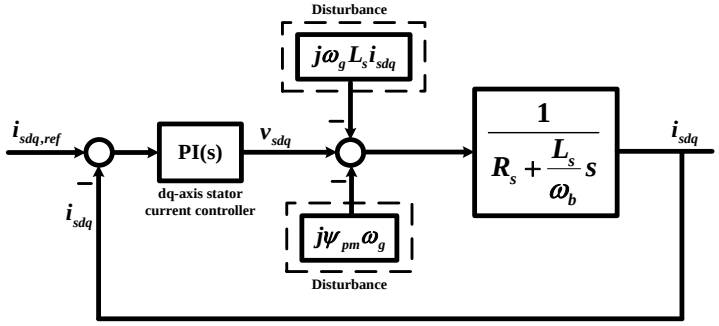

Fig. 4. Closed-loop control of dq-axes stator currents

The state equations corresponding to the stator current controllers are obtained as

$$\frac{dx_{i_{sd}}}{dt} = i_{sd,ref} - i_{sd} \tag{26}$$

$$\frac{dx_{i_{sq}}}{dt} = i_{sq,ref} - i_{sq} \tag{27}$$

3.1.2. dc-link voltage control by the MSC

Considering Fig. 1, the linearized power sharing equation in the dc-link section is given by [30]:

$$C_{dc}V_{dc_0}\frac{d\Delta V_{dc}}{dt} = -\Delta P_g - \Delta P_s - \Delta P_{loss} \tag{28}$$

Where P_g and P_{loss} represent the active power injected to the grid and power loss related to the generator, converter and interfaced filter, respectively, V_{dc} is the dc-link voltage, V_{dc_0} stands for the dc-link voltage at the operating point and C_{dc} is the dc-link capacitor. According to (21) and (28), the dc-link voltage is set to its reference voltage through q-axis stator current, i_{sq}. Fig. 5 depicts the closed-loop control of the dc-link voltage, where P_g and P_{loss} act as disturbances. The PI controller specifies the reference of the q-component stator current in ampere, $-I_{sq,ref}$, and to use it for the inner current loop, it has been converted to per unit through the gain $-1/I_B$, where I_B is the base current.

The state equations corresponding to the MSC outer dc-link voltage controller is obtained as

$$\frac{dx_{V_{dc}}}{dt} = V_{dc,ref} - V_{dc} \tag{29}$$

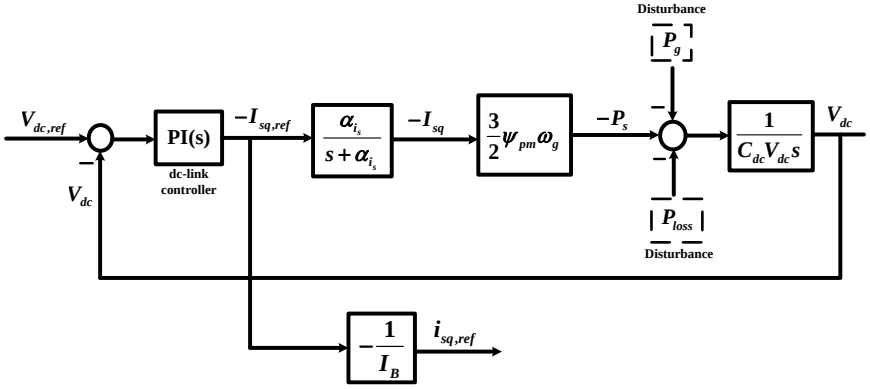

Fig. 5. Closed-loop control of the dc-link voltage

Figure 6 shows the overall block diagram of the MSC control system.

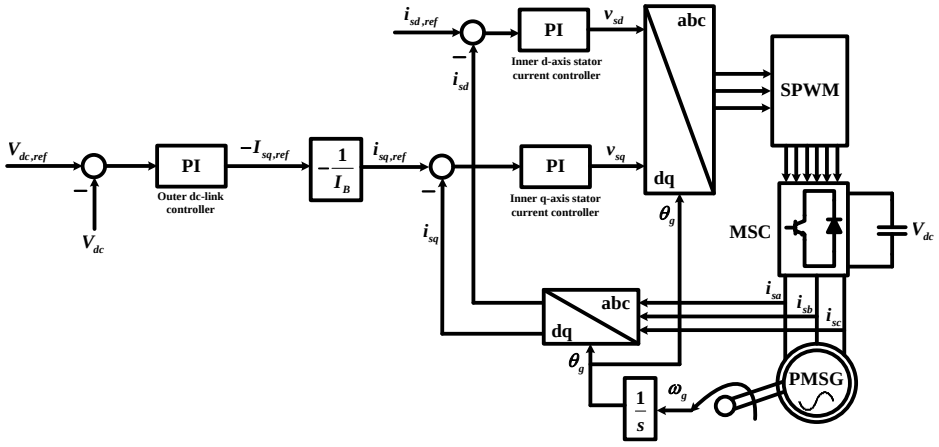

Fig. 6. Overall control structure of the MSC

3.2. Control structure of the Grid side converter

In this section, the control loops associated to the GSC is presented. The main function of the GSC in the power control mode is to control the active power injected to the grid. Further, the GSC can also regulate the power factor and reactive power injected to the grid. Similar to the MSC, the GSC control structure, consists of inner and outer loop controls.

3.2.1. GSC inner dq-axes current control loops

According to Fig. 1, the GSC voltage dynamics in pu and in the synchronous reference frame with grid voltage orientation ($v_{g,abc}$) can be written as

$$v_{cd} = R_g i_{gd} - L_g \omega i_{gq} + \frac{L_g}{\omega_B}\frac{di_{gd}}{dt} + v_{gd} \tag{30}$$

$$v_{cq} = R_g i_{gq} - L_g \omega i_{gd} + \frac{L_g}{\omega_B}\frac{di_{gq}}{dt} + v_{gq} \tag{31}$$

where i_{gd} and i_{gq} are the GSC dq-axes currents, v_{gd} and v_{gq} are the dq-components of the grid voltage, L_g and R_g are the inductance and resistance of the interfaced filter, in (p.u.), respectively, ω is the grid angular frequency obtained by the PLL, in rad/sec.

Figure 7 demonstrates the closed-loop control of the GSC dq-axes currents. The GSC is controlled in the dq-frame with grid voltage orientation, and thus, the d-axis reference current, $i_{gd,ref}$, is provided by the outer active power controller.

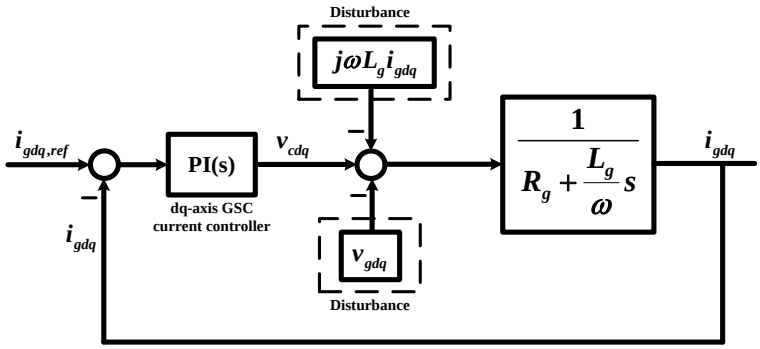

Fig7. GSC closed-loop current control loops

The state equations corresponding to the GSC dq-axes current controllers can be given as

$$\frac{dx_{i_{gdq}}}{dt} = i_{gdq,ref} - i_{gdq} \tag{32}$$

3.2.2. GSC outer active power control loop

Figure 8 depicts the closed-loop control of the GSC active power, where the reference active power $P_{g,ref}$ is determined based on a predefined power-speed curve designated based on aerodynamic specifications of the turbine blades. Generally, operating regions of the WT are the optimum and constant power modes. In the middle wind speed range, the output active power reference is set to the optimum value to yield a maximum power capture at a given wind speed. The relation between the active power reference and generator speed, ω_g, at the optimum state is approximated by $P_{g,ref}=k_{opt}\omega_g^3$, where at high wind speeds, the active power reference is limited to the rated value, i.e. 1 pu [3, 11]. The state equations corresponding to the GSC active power controller can be given as

$$\frac{dx_{P_g}}{dt} = P_{g,ref} - P_{g,ref} \tag{33}$$

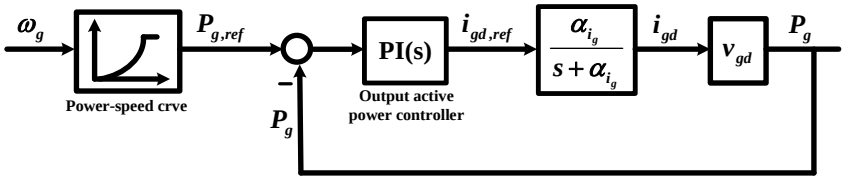

Fig. 8. GSC outer active power control loop

3.3. Pitch angle control loop

To prevent the mechanical fatigue loading or even the mechanical fails in the blades at above rated wind speeds, the pitch angle control system attempts to limit the WT aerodynamic power and consequently the generator speed to the their rated values. Figure 9 depicts the closed-loop control of the collective pitch angle system where $\omega_{g,ref}$ is the maximum operating of the generator speed, β_{ref} is the pitch angle command, β is the actual pitch angle and τ_β is the time constant of the pitch actuator. The saturation and rate limiter units are applied on the pitch angle command to set the maximum and minimum pitch angles and to regulate the rate of the pitch angle changes, respectively. Based on [31], considering the drive-train dynamics and the aerodynamic model uncertainties, the pitch angle controller parameters ($k_{P\text{-}\beta}$ and $k_{I\text{-}\beta}$) are obtained. The state equations related to the pitch system actuator and controller are obtained as

$$\frac{d\beta}{dt} = \frac{1}{\tau_\beta}(\beta_{ref} - \beta) \tag{34}$$

$$\frac{dx_\beta}{dt} = \omega_{g,ref} - \omega_g \tag{35}$$

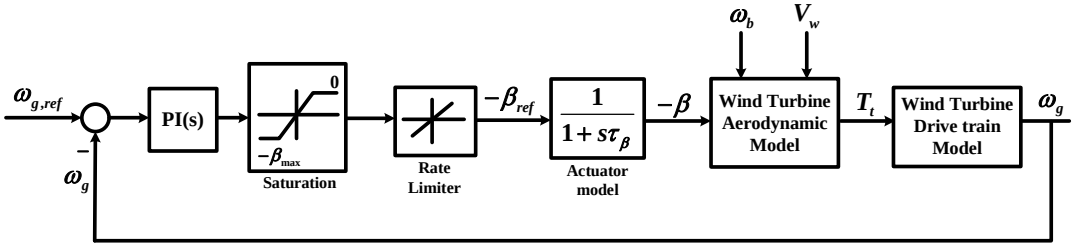

Fig. 9. Closed-loop control of the pitch angle

4. Small signal stability and modal analysis

Equations (8) – (15), (22) – (23) and (26) – (35) describe the dynamic electromechanical model of the WT and by linearizing and rearranging all of them, the linearized state space model of the WT system is obtained as

$$\Delta x^{\cdot} = A\Delta x + B\Delta u \tag{36}$$

where A is an 18×18 state matrix, x is the vector of state variables, x=[i_{sd}, $x_{i_{sd}}, i_{sq}, x_{i_{sq}}, i_{gd}, x_{i_{gd}}, i_{gq}, x_{i_{gq}}, x_{P_g}, V_{dc}, x_{V_{dc}}, \beta, x_\beta, \omega_g, \omega_b, \omega_h, \theta_{sh-bh}, \theta_{sh-hg}$]$^{\mathrm{T}}$, u is the vector of exogenous inputs, u=[$V_w, \omega_{g,ref}, v_g, V_{dc,ref}$]$^{\mathrm{T}}$, and B is the input matrix with adequate dimension. Modal analysis is carried out on the PMSG-based WT system with parameters of Appendix. The

system under study is an 8-pole, 5 MW, 690 V, 50 Hz PMSG-based WT system with rated wind speed of 12m/sec. The related parameters of the turbine and generator are shown in Appendix. Because the drive-train oscillatory modes at the constant power operation region of the power-curve are more intensively observable [4, 13], the operating points for this study are considered corresponding to the wind speed of 14 m/sec. Based on (36), the eigenvalues of the state matrix are obtained and then in order to disclose the relationship between the modes and state variables, the participation factors of state variables are calculated. In Table 1, the system eigenvalues, corresponding frequency and damping ratio and dominant state variables in the wind speed of 14m/sec are presented.

Table 1 Eigenvalues and dominant state variables for the study WT system

System Modes		Frequency (Hz)	Damping ratio	State variables with highest participation factor	
λ_1	-677.44	-	1	i_{sd}	
λ_2	-18.13	-	1	$x_{i_{sd}}$	
λ_3	–586.93	-	1	i_{sq}	
$\lambda_{4,5}$	-3.12 ± 83.87j	13.35	0.0372	θ_{sh-hg}	ω_h
$\lambda_{6,7}$	-45.92 ± 32.46j	5.17	0.82	V_{dc}	$x_{V_{dc}}$
λ_8	–18.18	-	1	$x_{i_{sq}}$	
$\lambda_{9,10}$	$-0.02 \pm 14.73j$	2.34	0.0014	θ_{sh-bh}	ω_g
λ_{11}	–9.05	-	1	β	
$\lambda_{12,13}$	$-0.76 \pm 0.46j$	0. 73	0.86	x_β	ω_b
λ_{14}	–62.83	-	1	x_{P_g}	
$\lambda_{15,16}$	$-628.32 \pm 0j$	-	1	i_{gd}	i_{gq}
$\lambda_{17,18}$	$-6.28 \pm 0j$	-	1	$x_{i_{gd}}$	$x_{i_{gq}}$

According to Table 1 and Section 2.2, the torsional modes $\lambda_{4,5}=-3.12\pm83.87j$, as the relatively weak damped modes, correspond to the shaft twist angle between the hub and generator $\theta_{sh\text{-}hg}$, and hub speed ω_h, with corresponding frequency and damping ratio of 13.35 Hz and 0.0372, respectively. In addition, the torsional modes $\lambda_{9,10}=-0.02\pm14.73j$, as the weakly damped modes are associated with the shaft twist angle between the blade and hub $\theta_{sh\text{-}bh}$, and generator speed ω_g with corresponding frequency and damping ratio of 2.34 Hz and 0.0014, respectively. Considering the dominant state variables of table 1, the modes $\lambda_{9,10}$, related to $\theta_{sh\text{-}bh}$ and ω_g, are known as blade in-plane modes that should be taken into account for reducing the blade in-plane fatigue loads. The real modes $\lambda_1=-677.44$, $\lambda_2=-18.13$, $\lambda_3=-586.93$, $\lambda_8=-18.18$, $\lambda_{11}=-9.05$ and $\lambda_{14}=-62.83$ are the very fast damped modes corresponding to i_{sd}, $x_{i_{sd}}$, i_{sq}, $x_{i_{sq}}$, β and x_{P_g}, respectively. The modes $\lambda_{6,7}=-45.92\pm32.46j$ are electrical fast modes correspond to the state variable V_{dc} with corresponding frequency and damping ratio of 5.17Hz and 0.82, respectively. The modes $\lambda_{12,13}=-0.76\pm0.46j$ correspond to the x_β and ω_b, and the modes $\lambda_{15,16}=-628.32\pm0j$ are very fast damped modes related to the i_{gd} and i_{gq}. From Table 1, the modes $\lambda_{4,5}$ and $\lambda_{9,10}$ are related to the drive-train

system with resonance frequencies of 13.34 Hz and 2.39 Hz, where the modes with frequency of 2.39Hz have lower damping ratio. Hence, once the modes $\lambda_{9,10}$ are excited, weakly damped oscillations appear on the blade-hub shaft torsional torque $T_{sh\text{-}bh}$, known as blade in-plane moment, causing the blade edgewise fatigue loads.

5. Proposed active method for mitigation of blade in-plane fatigue loading

According to the oscillatory torsional modes $\lambda_{4,5}$ and $\lambda_{9,10}$ in Table 1, the $\lambda_{9,10}$ modes have the least damping ratio and also the shaft twist angle between the blade and hub $\theta_{sh\text{-}bh}$ is the first dominant state variable with the highest participation factor. Considering (11), there is a significant correlation between $\theta_{sh\text{-}bh}$ and $T_{sh\text{-}bh}$, and hence by using (8) to (14), the shaft twist angle ($\theta_{sh\text{-}bh}$) dynamics can be described as a function of T_e and T_t, as follows:

$$\left[(K_{hg}+\frac{D_{hg}s}{\omega_B})(-1-\frac{\omega_B(K_{bh}+\frac{D_{bh}s}{\omega_B})}{2H_bs^2})+A+\frac{2H_gAs^2}{K_{hg}\omega_B+D_{hg}s}\right]\theta_{sh-bh}+$$
$$\left[\frac{\omega_B}{2H_bs^2}(K_{hg}+\frac{D_{hg}s}{\omega_B})+\frac{B(\omega_B(K_{hg}+\frac{D_{hg}s}{\omega_B})+2H_gs^2)}{K_{hg}\omega_B+D_{hg}s}\right]T_t+T_e=0 \quad (37)$$

where the polynomials A and B in (37) are obtained as

$$A=K_{hg}+\frac{D_{hg}}{\omega_B}s+\frac{2H_h}{\omega_B}s^2+\frac{1}{2H_bs}\left(\frac{K_{hg}\omega_B}{s}+D_{hg}+2(H_h+H_b)s\right)\left(K_{bh}+\frac{D_{bh}s}{\omega_B}\right)$$
$$B=1-\frac{1}{2H_bs}\left(\frac{K_{hg}\omega_B}{s}+D_{hg}+2(H_h+H_b)s\right) \quad (38)$$

Considering (38), (13) and (14), there is a direct relation between $d\theta_{sh\text{-}bh}/dt$ and (ω_b-ω_g). In other words, the fluctuations related to the blade in-plane modes originate from the speed difference between the blade and generator. Hence, if the electromagnetic torque has an auxiliary term proportional to (ω_b-ω_g), the blade in-plane fatigue loading can be effectively mitigated. Ignoring the generator losses, the relation between the PMSG electromagnetic torque and output active power can be described as

$$T_e\approx\frac{P_g}{\omega_g} \quad (39)$$

In Fig. 10, the proposed approach for active mitigation of blade in-plane fatigue loading is shown, in which, the supplementary term proportioned to (ω_b-ω_g) is added to $P_{g,ref}$, and thus the GSC output active power loop is modified. Therefore, according to (39), by modifying the GSC active

power control loop, the electromechanical torque contains the auxiliary term associated with (ω_b-ω_g) realizing active mitigation of the blade in-plane loads.

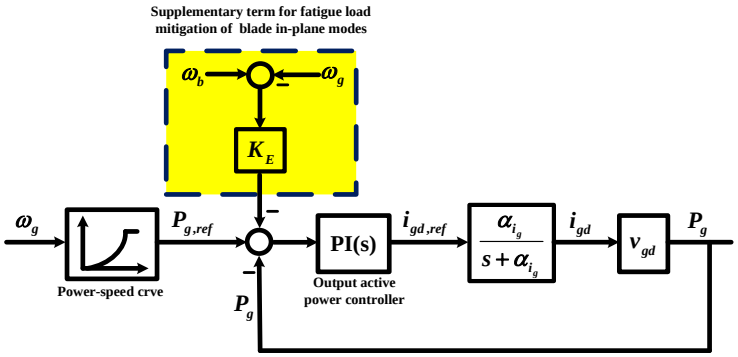

Fig. 10. The modified power control loop by applying the proposed supplementary term

Table 2 depicts the system eigenvalues and dominant state variables for the PMSG-WT system with modified output active power control loop and $K_E=10$. Comparing Tables 1 and 2, it is concluded that the proposed approach based on the modified power control loop significantly improves the damping ratio of the modes $\lambda_{9,10}$ from 0.0014 to 0.48.

Table 2: The eigenvalues and dominant state variables for the WT with proposed active mitigation method

System Modes		Frequency (Hz)	Damping ratio	State variables with highest participation factor	
λ_1	-677.44	-	1	i_{sd}	
λ_2	-18.13	-	1	$x_{i_{sd}}$	
λ_3	–586.6	-	1	i_{sq}	
$\lambda_{4,5}$	-2.61±84.83j	13.5	0.031	θ_{sh-hg}	ω_h
$\lambda_{6,7}$	-27.61 ± 32.55j	5.18	0.65	V_{dc}	$x_{V_{dc}}$
λ_8	-18.17	-	1	$x_{i_{sq}}$	
$\lambda_{9,10}$	$-7.76\pm14.26\,j$	2.27	0.48	θ_{sh-bh}	ω_g
λ_{11}	–9.45	-	1	β	
$\lambda_{12,13}$	$\lambda_{14}=-0.76\pm0.46\,j$	0.073	0.86	x_β	ω_b
λ_{14}	–84.93	-	1	x_{P_g}	V_{dc}
$\lambda_{15,16}$	-628.32±0j	-	1	i_{gd}	i_{gq}
$\lambda_{17,18}$	$\lambda_{17,18}=-6.28\pm0\,j$	-	1	$x_{i_{gd}}$	$x_{i_{gq}}$

5.1. Implementing the proposed approach for blade in-plane fatigue load mitigation

To implement the active mitigation approach proposed in section 5, access to estimated values of both the blade speed and generator speed is required. Because measuring the blade speed is not simply possible, in this section, the hub-generator and blade-hub torsional torques, i.e. $T_{sh\text{-}hg}$ and $T_{sh\text{-}bh}$, are firstly estimated, and then the blade speed is estimated. According to (11) to (14), (ω_b-ω_g) can be obtained as

$$\omega_b - \omega_g = \left(T_{sh-bh} + (\frac{K_{bh}}{K_{hg}} \frac{1}{1+sT_L} + \frac{D_{bh}}{D_{hg}} \frac{sT_{H1}}{1+sT_{H1}}) T_{sh-hg} \right) \frac{1}{D_{bh}} \frac{sT_{H2}}{1+sT_{H2}} \tag{40}$$

where the time constants T_L and T_{H1} are similar and can be given as $D_{hg}/K_{hg}\omega_B$, and time constant T_{H2} is $D_{bh}/K_{bh}\omega_B$. From (9)-(14), the torsional torques $T_{sh\text{-}hg}$ and $T_{sh\text{-}bh}$ can be described as

$$\bar{T}_{sh-hg} = -\bar{T}_e + 2H_g s\omega_g \tag{41}$$

$$\bar{T}_{sh-bh} = (1 + \frac{2H_h}{D_{hg}} s \frac{sT_{H2}}{1+sT_{H2}}) \bar{T}_{sh-hg} + 2H_h s\omega_g \tag{42}$$

where ω_g is the measured value of the generator speed by encoder sensor, $\bar{T}_{sh-hg}$ and $\bar{T}_{sh-bh}$ are the estimated values of the hub-generator and blade-hub torsional torques, respectively, $\bar{T}_e$ is the estimated value of the electromagnetic torque obtained through the output of the GSC outer loop controller. To prevent noise exposure of the generator speed, ω_g, the derivative operators in (41) and (42) must be replaced with the second order high pass filter, hence (41) and (42) are obtained as

$$\bar{T}_{sh-hg} = -\bar{T}_e + 2H_g \frac{s^2}{s^2 + 2\xi\omega_n s + \omega_n^2} \omega_g \tag{43}$$

$$\bar{T}_{sh-bh} = (1 + \frac{2H_h}{D_{hg}} \frac{s^2}{s^2 + 2\xi\omega_n s + \omega_n^2} \frac{sT_{H2}}{1+sT_{H2}}) \bar{T}_{sh-hg} + 2H_h \frac{s^2}{s^2 + 2\xi\omega_n s + \omega_n^2} \omega_g \tag{44}$$

where ω_n in (43) and (44) is the cut-off frequency of the high pass filters substituted with the derivative operators. The block diagram of Fig. 11 demonstrates the modified power control loop accomplished by the (40) and (43)-(44). It is noted that there is a dynamic interaction between the drive-train system and the control loops of the GSC and MSC.

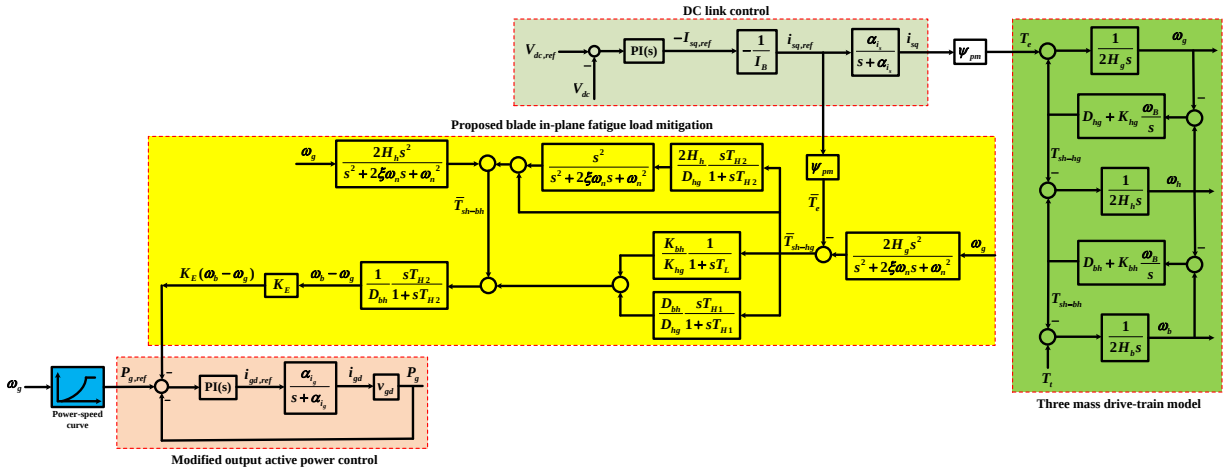

Fig. 11. Block diagram of the GSC modified power control loop with the proposed blade in-plane fatigue load mitigation

Figures 12 and 13 show the frequency responses of blade in-plane moment, $T_{sh\text{-}bh}$, to the wind speed, V_w, and grid voltage, v_g, for the PMSG WTs with and without the proposed compensator. According to Figs. 12 and 13, by using the modified power control loop, the amplitudes of the frequency responses of the blade-hub torsional torque to the both wind speed and grid voltage at the first drive-train resonance frequency significantly decrease. Hence, by employing the proposed compensator, fluctuations of the blade in-plane moment, under wind speed variation and grid voltage dip, are effectively improved.

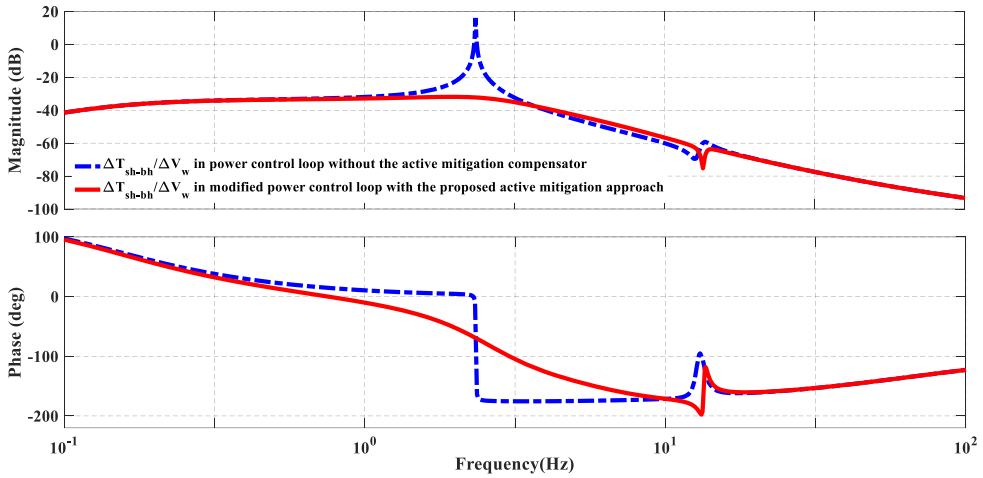

Fig. 12. Frequency response of the blade-hub torsional torque to the wind speed with and without the proposed fatigue load mitigation

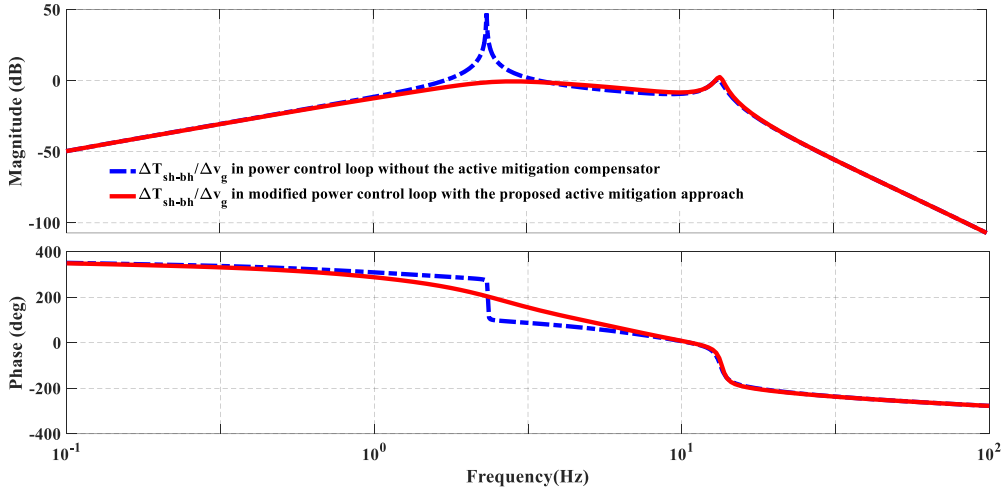

Fig. 13. Frequency response of the blade-hub torsional torque to the grid voltage with and without the proposed fatigue load mitigation

6. Simulation Results

In this section, at first, the dynamic capability of the proposed blade in-plane mitigation approach against the step change of the wind speed and grid voltage dip is examined. Then, the dynamic responses of the proposed approach are compared with those of the approaches based on the

generator speed feedback and the simplified two-mass drive train model. The simulation platform is established on the MATLAB Simulink environment. The study system, as shown in Fig. 1, consists of a 5MW, 690V, 50Hz PMSG-based WT connected to a 20kV distribution grid through a 10km-20kV cable and rated transformer.

6. 1. Performance evaluating of the proposed active mitigating approach

Figure 14 shows the time responses of the blade-hub shaft torsional torque and generator speed to the wind speed step change from 12m/s to 14m/s at the cases with and without the proposed blade in-plane mitigation approach. Moreover, Fig. 15 illustrate the frequency spectrum of blade in-plane shaft torsional torque and generator speed. Considering Figs. 14-15, after the step change of wind speed, in the case without the mitigation approach, the weakly damped oscillations with frequency of 2.34 Hz (related to the first resonance frequency $\omega_{01}=2\pi\times2.34$ *rad/sec*) are appeared on the blade-hub shaft torsional torque and generator speed. However, the fluctuations of the blade-hub shaft torsional torque are more severe than those of the generator speed that may result in stress and fatigue on the blades. According to Fig. 14, in the case with the proposed blade in-plane mitigation approach, the large oscillations associated with blade in-plane modes are effectively suppressed and the system quickly recovers its steady state. Besides, the frequency spectrums shown in Fig. 15 confirms the mitigation effect of the proposed approach. The simulation results in fig. 14 are in well agreement with the modal analysis results of Sections 4 and 5.

Figure 16 depicts the time response of the pitch angle for two cases with and without the proposed blade in-plane mitigation approach. Because of the interaction between the pitch control system and drive-train dynamics, after wind speed change, in the case without mitigation approach slight fluctuations related to blade in-plane modes appear on the pitch angle resulting in the increasing control effort of the pitch control system. Whereas by using the proposed mitigation approach, the mentioned fluctuations are quickly vanished.

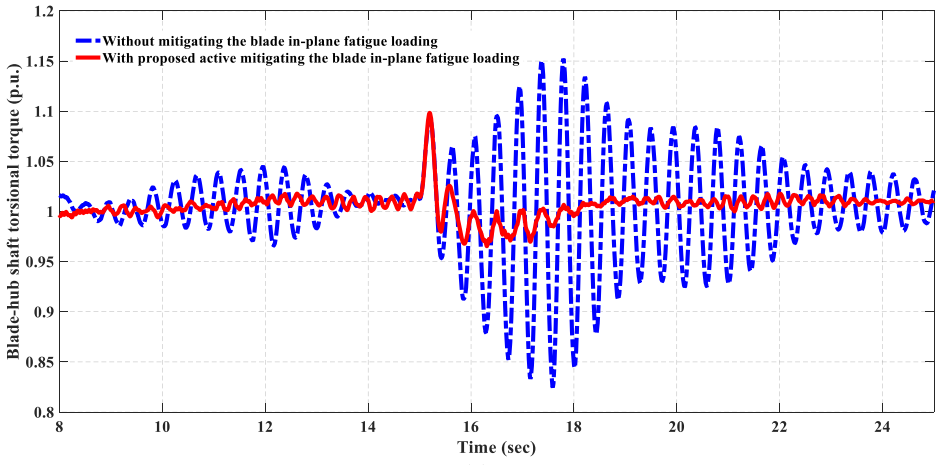

(a)

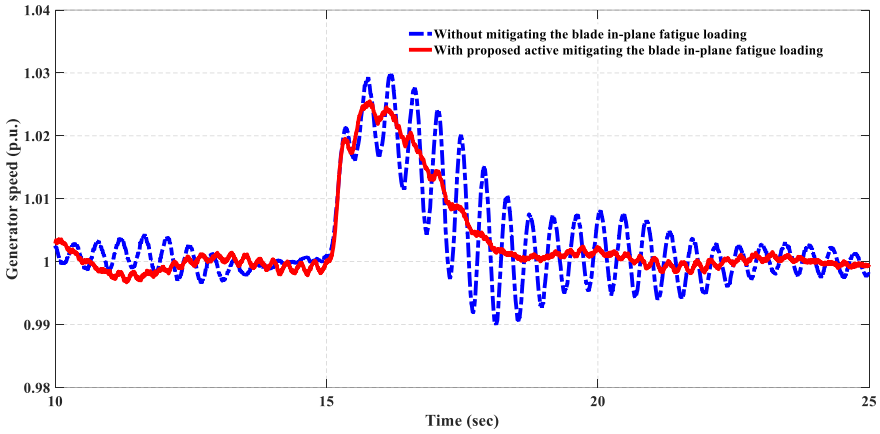

(b)

Fig. 14. Time responses of the blade-hub shaft torsional torque and generator speed to the step change of the wind speed for the cases with and without the blade-in plane mitigating approach

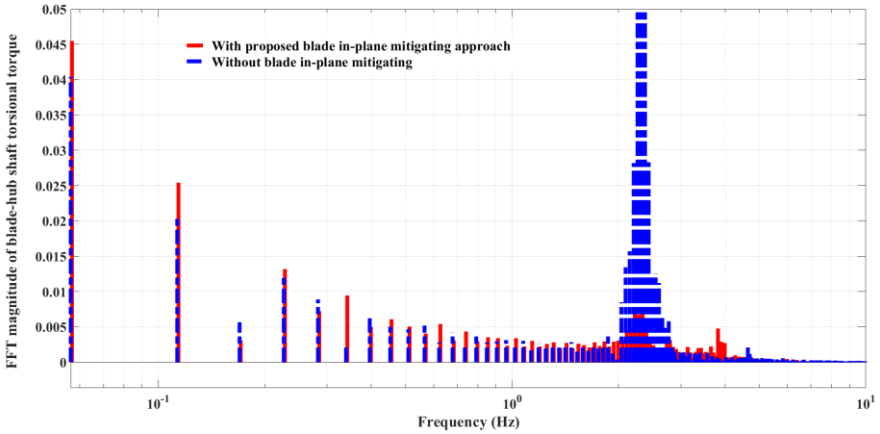

Fig. 15. Frequency spectrum of the blade-hub shaft torsional torque under the step change of the wind speed for the cases with and without the blade in-plane mitigating approach

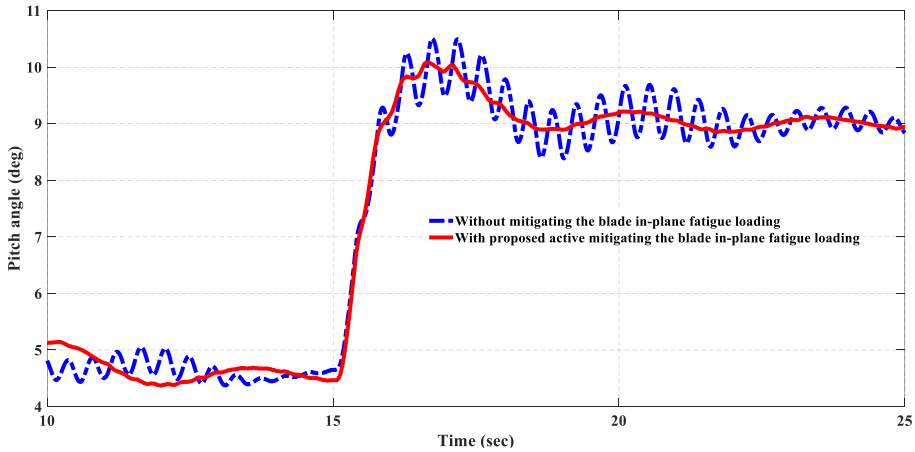

Fig. 16. Time responses of the pitch angle to the step change of the wind speed for the cases with and without the blade in-plane mitigation approach

Figures 17 demonstrates the waveforms of the actual and estimated blade-hub shaft torsional torque and blade speed once the proposed blade in-plane mitigation approach is applied and wind turbine is subjected to the wind speed step change. The estimated blade-hub shaft torsional torque and blade speed are extracted based on (40) and (44), respectively. It is clear that the estimated and actual waveforms coincide well with each other.

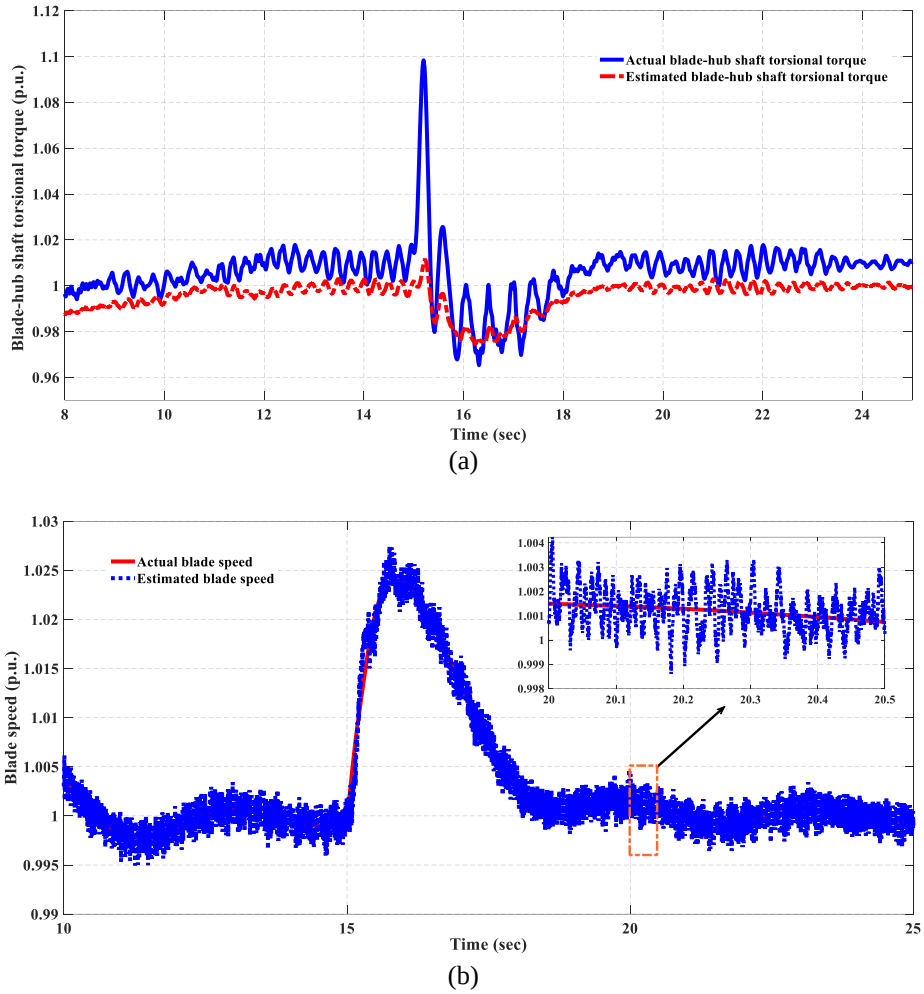

Fig. 17. Time responses of the actual and estimated blade-hub shaft torsional torque and blade speed to the step change of the wind speed by applying the proposed blade in-plane mitigation approach

Figure 18 exhibits time responses of the blade-hub shaft torsional torque and generator speed once WT is subjected to the grid fault at *t=15sec* for duration of 500msec. It is clear that in the case without the blade in-plane mitigation approach, weakly damped oscillations corresponding to blade in-plane loads appear on the wind turbine responses. Nevertheless, by employing the proposed blade in-plane mitigation approach, the blade in-plane oscillations are damped faster.

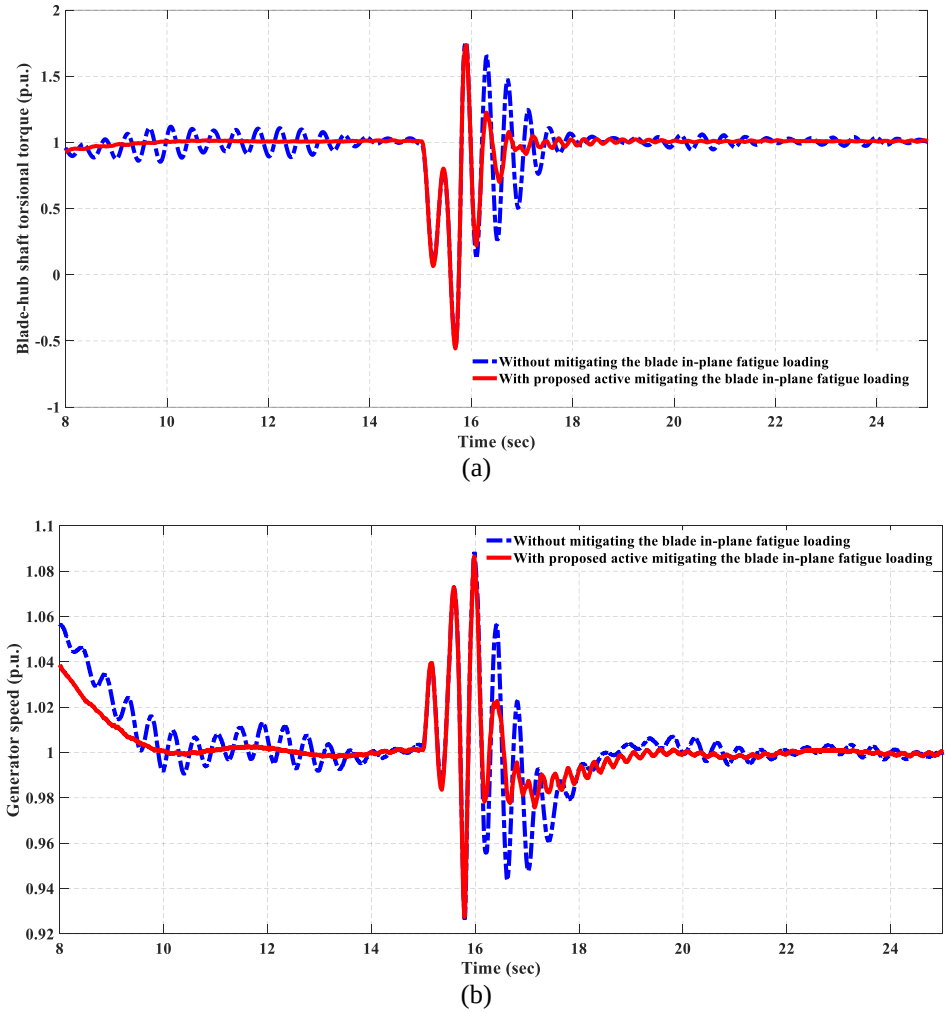

Fig. 18. Time responses of the blade-hub shaft torsional torque and generator speed to a grid voltage dip for the cases with and without the proposed blade-in plane mitigation approach

6. 2. Evaluating the borrowed mitigating approaches from torsional damping methods for blade in-plane fatigue load mitigation

In this section, two other approaches for suppressing the blade in-plane fatigue loads are presented. These approaches are borrowed from torsional damping methods reviewed in the literature. First approach is realized by modifying the power reference via the generator speed feedback and passing it through a BPF. The second approach is realized by using the speed difference between the turbine and generator based on the simplified two-mass drive-train model.

6. 2. 1. Blade in-plane fatigue load mitigation by using the generator speed feedback

Figure 19 depicts the control structure of the modified power control loop made by the feedback of the generator speed and passing it through BPF. The BPF extracts the oscillatory blade in-plane fluctuations from the generator speed, and therefore, the drive-train resonance peaks are attenuated.

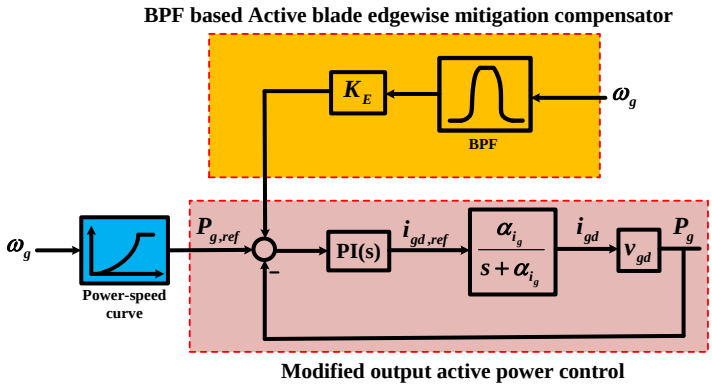

Fig. 19. Modified power control loop created by the feedback of the generator speed and passing it through BPF

Figures 20 and 21 show frequency responses of the $T_{sh\text{-}bh}$ to the wind speed, V_w, and grid voltage, v_g, at three cases, where the first and second cases are associated with the proposed damping approach and the damping approach based on the generator speed feedback, respectively, and in the third case no damping approach is employed. According to Figs. 20 and 21, by using the proposed active mitigation approach, the amplitudes of frequency responses at the first resonance frequency considerably decreased, resulting in significant positive damping action on torsional oscillations.

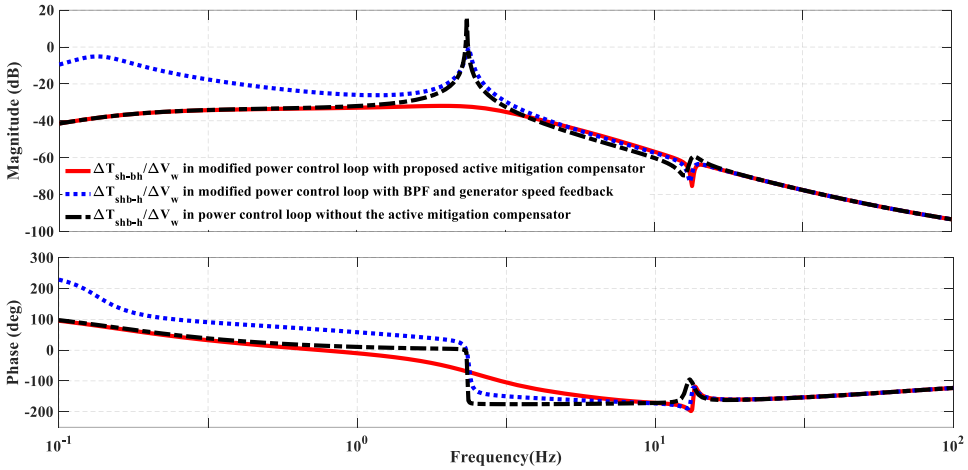

Fig. 20. Frequency response of $T_{sh\text{-}bh}$ to the wind speed at three cases corresponding to the proposed active mitigation approach, damping approach based on the generator speed feedback and no damping approach

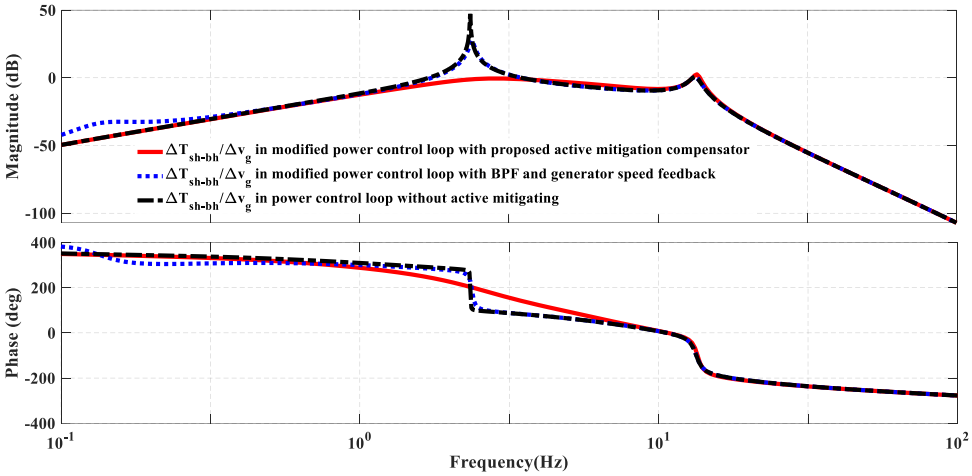

Fig. 21. Frequency response of $T_{sh\text{-}bh}$ to the grid voltage at three cases corresponding to the proposed active mitigation approach, damping approach based on the generator speed feedback and no damping approach

6. 2. 2. Blade in-plane fatigue load mitigation by employing the (ω_t-ω_g) term based on the simplified two-mass drive-train model

Considering the three-mass drive-train model, the hub-generator shaft has the lower stiffness coefficient and is more flexible compared to the blade-hub shaft. Therefore by neglecting the blade-hub shaft in the three-mass drive-train model, the simplified drive-train model can be obtained, known as the two-mass drive-train model. Hence, based on the two-mass drive-train model, the proposed blade in-plane fatigue load mitigation approach given in in Section 5 can be implemented. The term ω_t-ω_g, as the difference of the turbine and generator speeds, by using the two-mass drive-train model can be obtained as

$$(\omega_t - \omega_g) = \frac{1}{D_{hg}} \frac{sT_H}{1+sT_H} (-\bar{T}_e + \frac{2H_g s}{1+sT_D} \omega_g) \tag{45}$$

where ω_t is the angular speed related to the turbine hub and blades, and the time constants T_H and T_D are $D_{hg}/K_{hg}\omega_B$ and $1/\omega_n$, respectively. Fig. 22 depicts the block diagram of the modified power control loop via the (ω_t-ω_g) compensator taken from the two-mass drive-train model. In the next Section, performance of this method is surveyed and is compared with that of the proposed blade in-plane fatigue load mitigation approach.

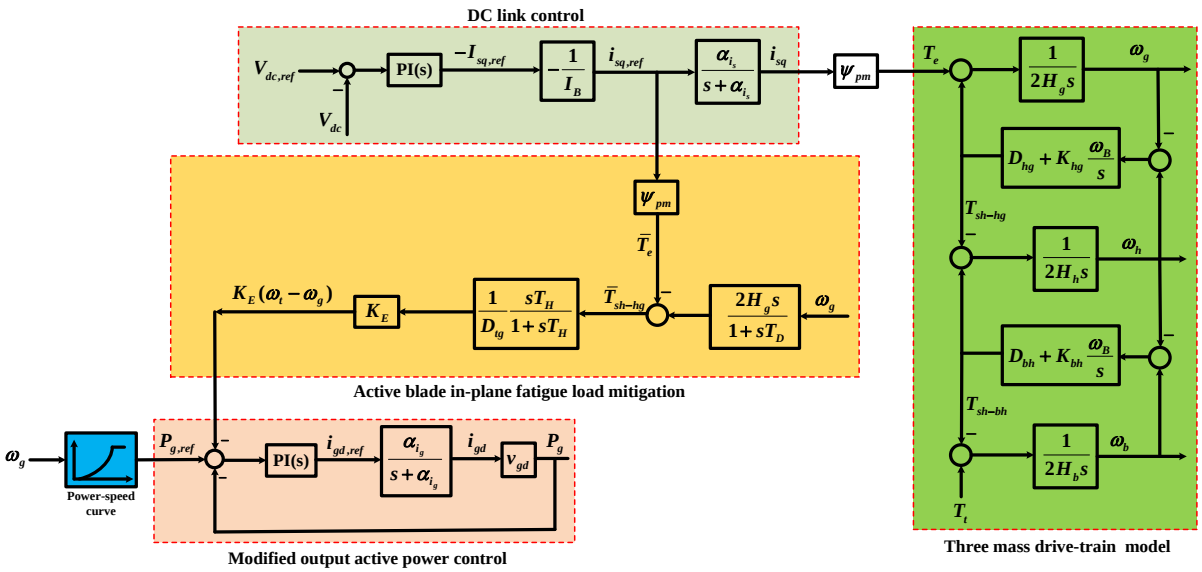

Fig. 22. Implementing the blade in-plane active mitigation compensator based on the simplified two-mass drive-train model

6. 2. 3. Performance comparison of the proposed blade in-plane mitigation approach and the approaches based on the generator speed feedback and employing the (ω_t-ω_g) term

Figures 23 and 24 depict the time responses of the blade-hub shaft torsional torque and generator speed against step change of wind speed and grid voltage dip at four different cases, first case: without damping approach, second case: proposed mitigation approach, third case: approach based on the generator speed feedback, fourth case: approach based on simplified two-mass drive-train model. Considering Figs. 23 and 24, it is evident that the proposed approach has the most efficient in suppression of oscillations appeared on the blade-hub shaft torsional torque and generator speed.

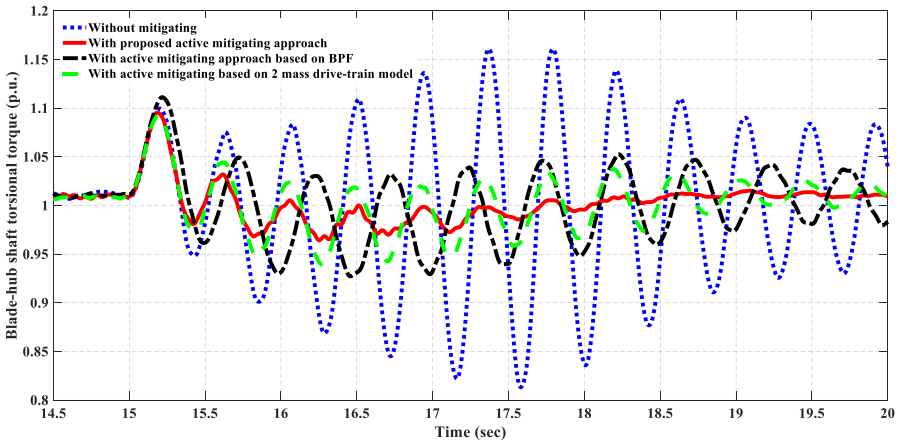

(a)

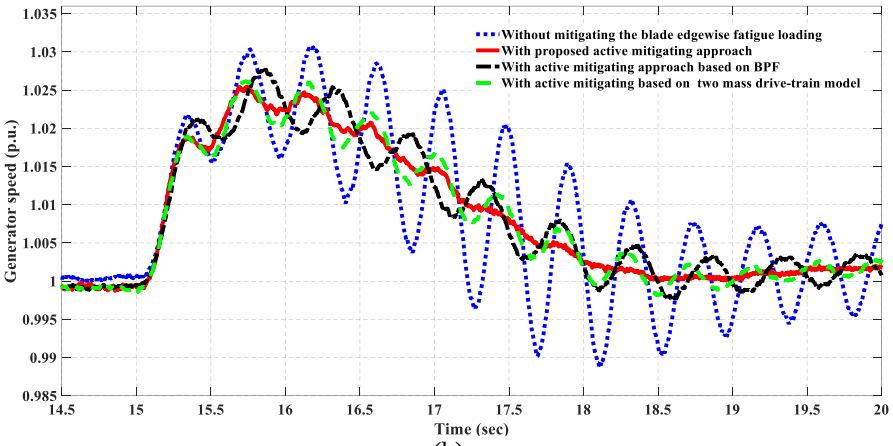

(b)

Fig. 23. Time responses of the blade-hub shaft torsional torque and generator speed to the step change of the wind speed at different cases

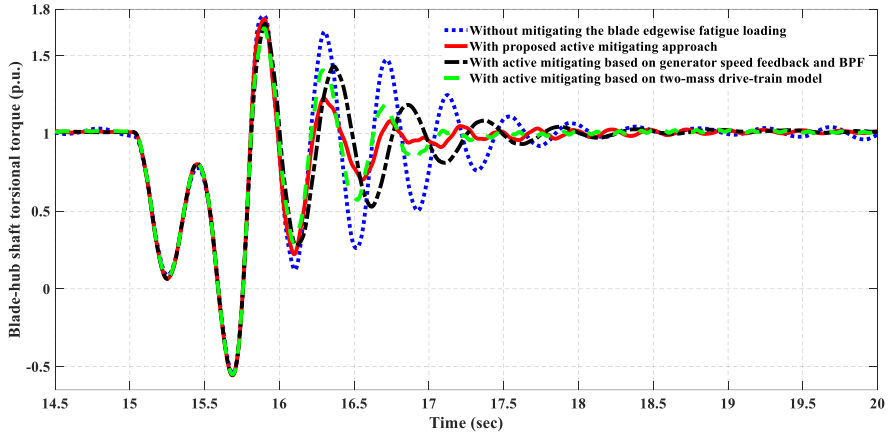

(a)

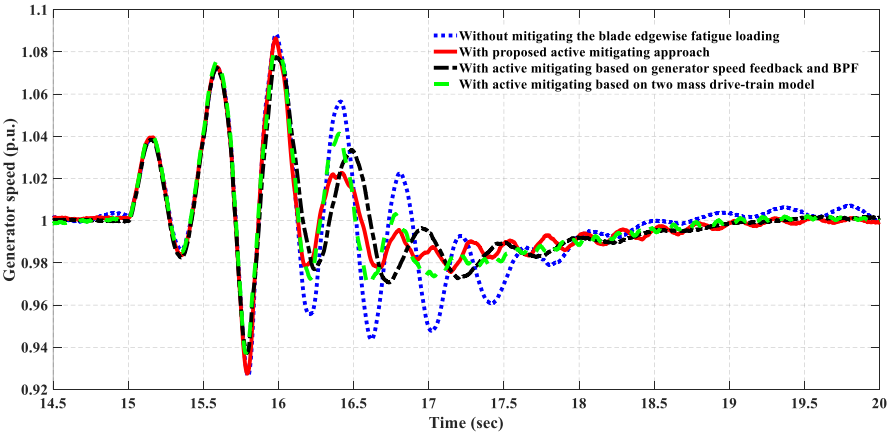

(b)

Fig. 24. Time responses of the blade-hub shaft torsional torque and generator speed against the grid voltage dip at different cases

7. 3. Impact of shaft stiffness estimation error on performance of the proposed approach

In this Subsection, the capability of the proposed blade in-plane mitigation approach in presence of shaft stiffness estimation error is assessed and compared with other approaches. Considering (16) and (17), the drive-train resonance frequencies are affected by both the stiffness coefficients of the blade-hub and hub-generator shafts. Figures 25 and 26 show time responses of the blade-hub shaft torsional torque and generator speed against the step change of the wind speed. In Fig. 25, -15% error and in Fig. 26, +15% error are considered in estimation of shaft stiffness coefficients. According to Figs. 25 and 26, the proposed mitigation approach performs well in suppression of blade in-plane oscillations even under uncertainty in estimation of shaft stiffness coefficients.

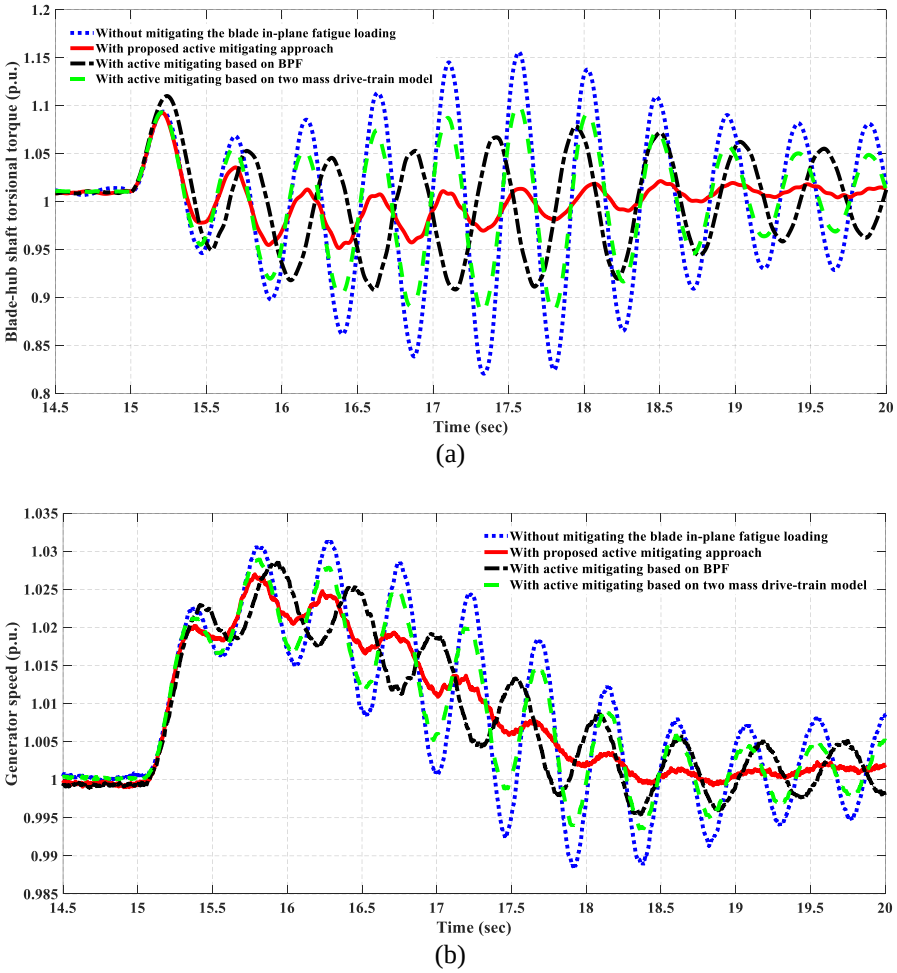

Fig. 25. Time responses of the blade-hub shaft torsional torque and generator speed against the step change of the wind speed under -15% error in estimation of shaft stiffness coefficients

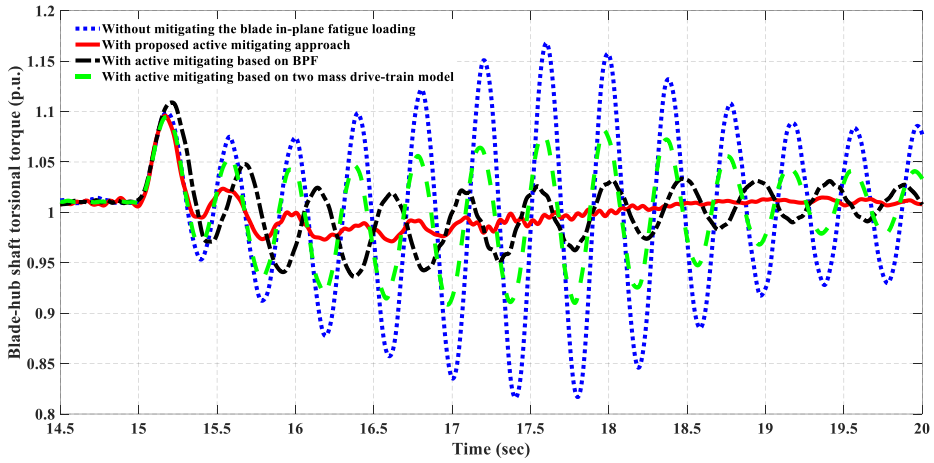

(a)

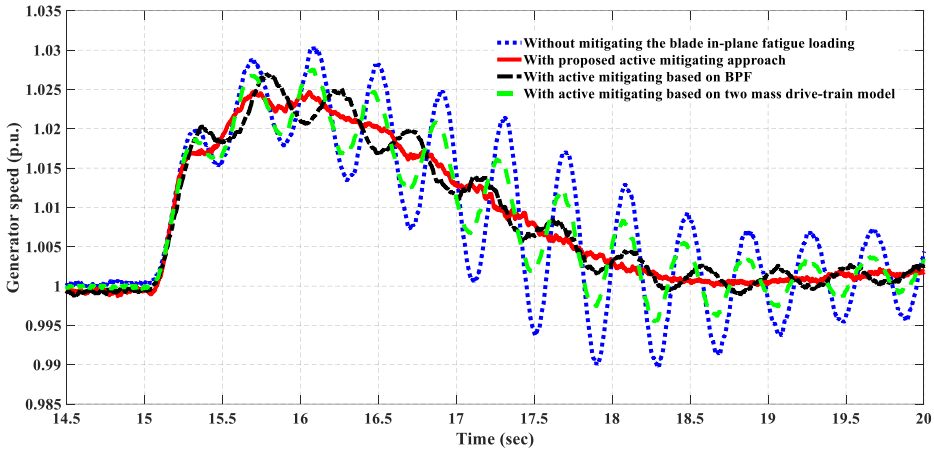

(b)

Fig. 26. Time responses of the blade-hub shaft torsional torque and generator speed against the step change of the wind speed under +15% error in estimation of shaft stiffness coefficients

7. 4. Performance of the proposed mitigation approach considering blade passing phenomenon

Figure 27 depicts the time responses of the blade-hub shaft torsional torque and generator speed to step change of wind speed under BPPh and for different mitigating strategies. Considering Fig. 27, the proposed mitigating approach even under BPPh has appropriate performance as well as has superior effect over than 2 other mitigating approaches.

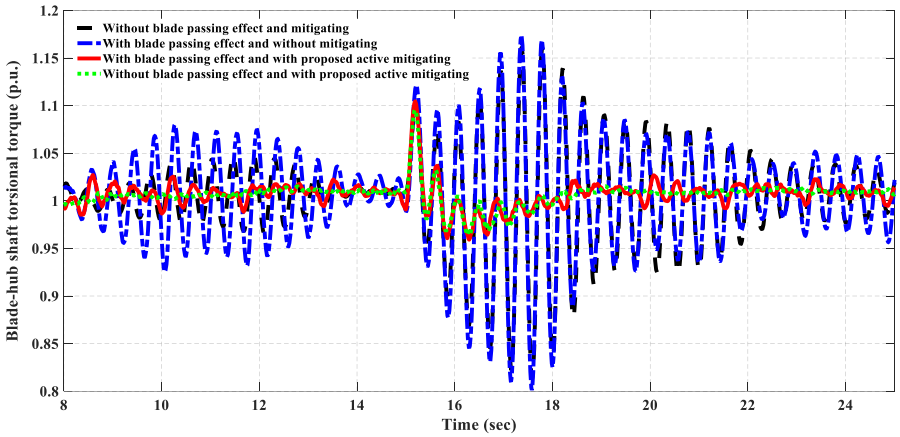

(a)

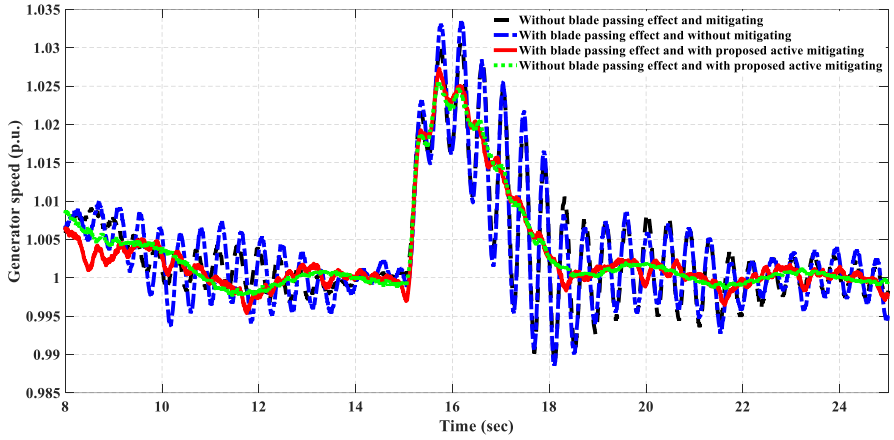

(b)

Fig. 27. Time responses of the blade-hub shaft torsional torque and generator speed to the step change of the wind speed under BPPh

8. Conclusion

This paper focuses on active mitigation of the blade in-plane fatigue loading in megawatt-scale grid connected PMSG-based WT. For this, at first, the drive-train model is such considered that the blade in-plane oscillatory modes that are responsible for blade in-plane fatigue loads can be accurately extracted. And then, by using the small signal stability analysis, the dynamic performance of the WT is examined. Modal analysis exhibits that if any damping action is not considered in the control system, the open-loop oscillatory modes with low damping ratio appear on the blade-hub shaft torsional torque as the closed-loop system modes. These modes could result in appearing low-frequency oscillations on the blade-hub shaft torsional torque once subjecting the electrical or mechanical excitations which can compromise the reliability of the WT blades.

To mitigate the blade in-plane fatigue loading, this paper proposes a mitigation approach implemented by modifying the power control loop, indeed a damping auxiliary term is added into the electromagnetic torque. This component is proportional to the speed difference between the blade and generator. It is shown that the proposed approach effectively alleviates the blade in-

plane fatigue loading, moreover, it has superior efficacy over two other mitigating approaches borrowed from torsional damping methods in the literature under several case studies.

References

[1] I. P. Girsang, J. S. Dhupia, E. Muljadi, M. Singh and J. Jonkman, "Modeling and Control to Mitigate Resonant Load in Variable-Speed Wind Turbine Drivetrain," *IEEE Journal of Emerging and Selected Topics in Power Electronics*, vol. 1, no. 4, pp. 277-286, Dec. 2013.

[2] A. Beiki and M. Rahimi, "An efficient sensorless approach for energy conversion enhancement and damping response improvement in permanent magnet synchronous generator (PMSG) based wind turbines", *Int. Trans. Electr. Energy Syst.*, vol. 29, no. 1, 2019.

[3] M. Rahimi, "Mathematical modeling dynamic response analysis and control of pmsg-based wind turbines operating with an alternative control structure in power control mode", *International Transactions on Electrical Energy Systems*, vol. 27, no. 12, pp. e2423, 2017.

[4] M. Rahimi, "Improvement of energy conversion efficiency and damping of wind turbine response in grid connected DFIG based wind turbines", *Int. J. Electr. Power Energy Syst.*, vol. 95, pp. 11-25, Feb. 2018.

[5] M. D. Reder, E. Gonzalez and J. J. Melero, "Wind turbine failures-tackling current problems in failure data analysis", *Proc. J. Phys. Conf.*, vol. 753, 2016.

[6] O. Anaya-Lara, N. Jenkins, J. Ekanayake and P. Cartwright, Wind Energy Generation: Modelling and Control, Hoboken, NY, USA:Wiley, 2009.

[7] H. Liu, Q. Tang, Y. Chi, Z. Zhang, and X. Yuan, "Vibration reduction strategy for wind turbine based on individual pitch control and torque damping control", *Int. Trans. Electr. Energ. Syst.*, vol. 26, pp. 2230-2243, Oct. 2016.

[8] Y. Zhang, D. Xie, J. Feng and R. Wang, "Small-signal modelling and modal analysis of wind turbine based on three-mass shaft model", *Electr. Power Compon. Syst.*, vol. 42, pp. 693-702, Apr. 2014.

[9] H. Li and Z. Chen, "Transient stability analysis of wind turbines with induction generators considering blades and shaft flexibility", *IECON 33rd Annual Conference of the IEEE Industrial Electronics Society*, pp. 1604-1609, 2007.

[10] V. P. Singh, N. Kishor, P. Samuel and N. Singh, "Small-signal stability analysis for two-mass and three-mass shaft model of wind turbine integrated to thermal power system", *Comput. Elect. Eng.*, vol. 78, pp. 271-287, Sep. 2019.

[11] M. Rahimi, A. Beiki, "Efficient modification of the control system in PMSG-based wind turbine for improvement of the wind turbine dynamic response and suppression of torsional oscillations," *Int. Trans. Electr. Energy Syst*, vol. 28, no. 8, pp. 2578, Aug. 2018.

[12] Feng Xie and Aly-Mousaad Aly, "Structural control and vibration issues in wind turbines: A review", *Engineering Structures*, vol. 210, no. 2020, pp. 110087, May. 2020.

[13] J. Licari, C. E. Ugalde-Loo, J. Liang, J. Ekanayake and N. Jenkins, "Torsional damping considering both shaft and blade flexibilities", *Wind Eng.*, vol. 36, no. 2, pp. 181-195, Apr. 2012.

[14] T. Ackermann, Wind Power in Power System, Hoboken, NJ, USA:Wiley, 2012.

[15] J. M. Jonkman, S. Butterfield, W. Musial and G. Scott, Definition of a 5-MW Reference Wind Turbine for Offshore System Development, Golden, CO, USA:National Renewable Energy Laboratory, 2009.

[16] J. K. Kambrath, M. S. U. Khan, Y. Wang, A. I. Maswood and Y. J. Yoon, "A novel control technique to reduce the effects of torsional interaction in wind turbine system", *IEEE J. Emerg. Sel. Topics Power Electron.*, vol. 7, no. 3, pp. 2090-2105, Sep. 2019.

[17] Z. Li, S. Tian, Y. Zhang, H. Li and M. Lu, "Active control of drive chain torsional vibration for DFIG-based wind turbine", *Energies*, vol. 12, no. 9, pp. 1744, May 2019.

[18] Y. Wang, Y. Guo, D. Zhang, H. Liu and O. Song, "Analysis and mitigation of the drive train fatigue load for wind turbine with inertial control, "*International Journal of Electrical Power & Energy Systems*, vol. 136, pp. 107698, March. 2022.

[19] E.L. van der Hooft, P. Schaak, and T.G. van Engelen. Wind turbine control algorithms. ECN DOWEC-F1W1-EH-03-094/0, Petten, The Netherlands, 2003.

[20] A. G. Abo-Khalil, S. Alyami, K. Sayed and A. Alhejji, "Dynamic modeling of wind turbines based on estimated wind speed under turbulent conditions", *Energies*, vol. 12, no. 10, pp. 1907, May 2019.

[21] D. S. L. Dolan and P. W. Lehn, "Simulation model of wind turbine 3p torque oscillations due to wind shear and tower shadow", *IEEE Trans. Energy Convers.*, vol. 21, no. 3, pp. 717-724, Sep. 2006.

[22] O. Anaya-Lara, N. Jenkins, J. Ekanayake and P. Cartwright, Wind Energy Generation: Modelling and Control, Hoboken, NY, USA:Wiley, 2009.

[23] J. Licari, *Control of a Variable-Speed Wind Turbine*, 2013.

[24] E. A. Bossanyi, "Wind turbine control for load reduction", *Wind Energy*, vol. 6, no. 3, pp. 229-244, 2003.

[25] A. D. Hansen and G. Michalke, "Modelling and control of variable speed multi-pole permanent magnet synchronous generator wind turbine", *Wind Energy*, vol. 11, no. 5, pp. 537-554, 2008.

[26] P. N. Paraskevopoulos, Modern Control Engineering, Boca Raton, FL, USA:CRC Press, 2017.

[27] L. Liu, D. Xie, H. Chu and C. Gu, "A damping method for torsional vibrations in a DFIG wind turbine system based on small-signal analysis", *Electric Power Compon. Syst.*, vol. 45, no. 5, pp. 560-573, Mar. 2017.

[28] L. Liu and D. Xie, "Performance comparison of two different filter design approaches for torsional vibration damping in a doubly fed induction generator-based wind turbine", *J. Eng.*, vol. 2015, no. 6, pp. 197-204, Jun. 2015.

[29] M. Rahimi, "Modeling control and stability analysis of grid connected PMSG based wind turbine assisted with diode rectifier and boost converter", *Int. J. Electr. Power Energy Syst.*, vol. 93, pp. 84-96, Dec. 2017.

[30] A. Safaeinejad, M. Rahimi, "Control and performance analysis of grid-connected variable speed wind turbine with dual stator-winding induction generator for the contribution of both stator windings in active power transmission", *IET Renewable Power Generation*, vol. 14, pp. 2348-2358, Oct. 2020.

[31] M. Rahimi and M. Asadi, "Control and dynamic response analysis of full converter wind turbines with squirrel cage induction generators considering pitch control and drive train dynamics", *Int. J. Electr. Power Energy Syst.*, vol. 108, pp. 280-292, Jun. 2019.

Appendix A

Specifications of wind turbine model

Symbol	Quantity	Value
P_n	Rated output power	5 MW
R	Blade radius	63 m
n_g	Gearbox ratio	62
ρ	Air density	1.222 kg/m^3
J_b	Blade moment of inertia	2.84×10^7 kgm^2
J_h	Hub moment of inertia	753519 kgm^2
H	Hub height	90 m
$K_{sh\text{-}bh}$	Blade-hub shaft stiffness coefficient	6.6×10^8 N.m/rad
$K_{sh\text{-}hg}$	Hub-generator shaft stiffness coefficient	3.66×10^9 N.m/rad
D_{bh}	Mutual damping coefficient between the blades and hub	1.56×10^6 N.m.sec/rad
D_{hg}	Mutual damping coefficient between the hub and generator	1.05×10^6 N.m.sec/rad
a	Tower radius	2.4 m
α	Wind shear component	0.3
X	Blade origin from tower midline	5 m
τ_β	Time constant of the pitch actuator	0.1 sec
ω_{b_B}	Base angular frequency of the blades	$0.4032\times\pi$ rad/sec

Appendix B

Specifications of PMSG

Symbol	Quantity	Value
S_b	Rated output power	5 MVA
V_b	Rated voltage	690 V
n_p	Pole pairs	4
ω_B	Base angular electrical frequency	$100\times\pi$ rad/sec
J_g	Generator moment of inertia	2.12×10^{6} kgm^2
R_s	Stator resistance	8.28×10^{-4} Ω
L_s	Stator inductance	4.091×10^{-5} H
ψ_{pm}	Permanent magnet flux linkage	1.7036 Wb